Korean J. Chem. Eng., 39(2), 451-459 (2022)
DOI: 10.1007/s11814-021-0934-x

pISSN: 0256-1115
eISSN: 1975-7220

Digital light processing 3D printing of multi-materials with improved adhesion using resins containing low functional acrylates

Hyeonwoo Hwangbo and Seog-Jin Jeon†

Department of Polymer Science and Engineering, Kumoh National Institute of Technology, Gumi, Gyeongbuk 39177, Korea
(*Received 13 May 2021 • Revised 2 August 2021 • Accepted 19 August 2021*)

Abstract−Digital light processing (DLP) 3D printing has received increasing attention due to high-resolution printing capability, mass productivity, and cheap equipment cost. Most of all, the layer resolution less than 50 μm overwhelms 200-300 μm layer resolution of its competitive technology, filament deposition modeling (FDM) 3D printing. Despite the advantage of the high resolution, weak mechanical properties of DLP 3D printouts have limited their industrial use. One of the easiest ways to improve mechanical property is the use of multi-materials that complement each other's weak property. However, DLP 3D printing of multi-material printouts with reliable adhesion has been largely unexplored. In this study, we compared the mechanical properties of four pairs of multi-materials consisting of two different materials of the same thickness. A composition with highest modulus and ultimate strength was fixed as the first half layer, and the acrylate of the composition for the other half layer was modulated with a monomer having a functionality between 1 and 3. If the acrylate monomer's functionality for the other half layer was less than three, the multi-material printout showed nearly averaged mechanical property of each material. We speculate that low functional acrylate with lower viscosity allows sufficient polymerization at the interface, enabling reliable adhesion. This approach that enables successful multi-material printing with improved adhesion and complementary mechanical properties will extend the use of DLP 3D printing in a broad range of industrial application that requires both sophisticated shape and mechanical strength.

Keywords: Digital Light Processing 3D Printing, Functionality, Multi-material

INTRODUCTION

The facile and customizable manufacturing ability of 3D printing has attracted much attention from personal to industrial areas [1-3]. While personal uses are mainly for aesthetic purposes, including modeling and prototyping, which do not require high mechanical strength, the industrial application requires high modulus, tensile strength, and elongation at break. Since this requirement is often difficult to achieve with a single material, there is a need for multi-materials with reliable adhesion [4,5]. In addition, emerging technologies based on 3D printing such as bio-printing [6,7] and 4D printing [8,9] basically require multi-material printing.

The most advanced method for multi-material printing is material jetting (MJ) [10,11]. MJ enables printing of sophisticated multi-material 3D structures by spraying multiple photo-curable materials and subsequent UV exposure. However, since UV-curable ink with a composition not optimized for surface tension and viscosity can permanently damage the printer due to nozzle clogging, the research was mainly led by the printer manufacturer. In addition, due to the locked-down information about the device and commercial inks by the patent holder, only little study has been published for multi-material MJ printing [12,13]. On the other hand, fused deposition modeling (FDM) 3D printing has been largely studied because of disclosed information about materials and inexpensive equipment cost [14,15]. However, reliable adhesion between multi-materials is not achieved by simple fusion [16-18]. Direct ink writing (DIW), a similar extrusion-based method but uses fluid ink, exhibits better adhesion than FDM by using covalent bonds between thermoset polymers [19-22]. However, deformation due to oozing significantly reduces printing quality.

Digital light processing (DLP) 3D printing has the advantage of obtaining higher resolution in a shorter time than the extrusion-based 3D printing methods [23-26]. Typical layer resolution is less than 50 μm, which is at least four-times smaller than that of the extrusion-based 3D printing, 200-300 μm. This difference is critical considering that the pixel size of the most recent cell phones' display is about 80 μm, based on the smallest size that can be resolved by the human eye. The variety of applicable materials and available cross-linking pathways are another advantage. Mechanical properties can be widely controlled by a combination of photo-curable materials, e.g., acrylates, and by applying more than two polymerization pathways among radical, thiolene, and cationic polymerization [3,23,24]. But, in the case of multi-material printing, studies have been mainly conducted for systems composed of chemicals with the same or similar chemical structures but with different mixing ratios to achieve reliable adhesion [27-31]. For example, Borrello et al. controlled the ratio of monomer and cross-linker from 1 : 0 to 1 : 1, thereby controlling the modulus in the range of 0.6-31 MPa [27]. They performed multi-material printing of low and high modulus resin compositions, but not provided mechanical properties. On the other hand, only a few studies have been made for multi-material DLP 3D printing using chemically different com-

†To whom correspondence should be addressed.
E-mail: sjjeon@kumoh.ac.kr

positions. Recently, Zhang et al. performed multi-material printing of hydrogel and elastomer, and obtained a hybrid characteristic of high modulus and high elongation [32]. Low elastic modulus materials such as hydrogel and elastomer under the Dahlquist criterion ($G'<10^5$ Pa) are known to have good adhesion characteristics [33]. For materials exceeding the Dahlquist criterion, the interfacial adhesion of printed multi-materials using resins composed of chemically different substances was largely unexplored.

Here, we introduce a method of obtaining complementary mechanical properties through multi-material DLP 3D printing. We show 3D printing results of photo-curable resins containing monomers with different functionality, and suggest the relationship between the functionality of the monomer and the mechanical properties of the multi-material printouts. We found that the multi-material printouts have complementarily reinforced mechanical properties of constituent materials, if the functionality of monomer in the resin composition to be printed on a pre-printed layer is less than three. Finally, multi-material printing of high modulus and the high elongation resin compositions was successfully performed, and the composite properties of the printouts were confirmed. We expect that this approach will enable sophisticated control of mechanical properties of 3D printouts required for industrial applications. In addition, combinatorial advantages of high layer resolution and precisely controlled mechanical properties will greatly enhance the use of DLP 3D printing in various industrial applications.

MATERIALS AND METHODS

1. Materials

Difunctional urethane acrylate oligomer (UA, molecular weight 2,000 g/mol) was purchased from Sartomer. Pentaerythritol tetraacrylate (PETA), ethoxylated trimethylolpropane triacrylate (ETPTA), dipropylene glycol diacrylate (DPGDA), and isobornyl acrylate (IBA) were provided as free samples from Sartomer. Trimethylolpropane triacrylate (TMPTA) and hydroxybutyl acrylate (HBA) were purchased from TCI chemicals. Phenylbis(2,4,6-trimethylbenzoyl)phosphine oxide (BAPO) and 2,5-Bis(5-tert-butyl-2-benzoxazoyl)thiophene (TBT) were purchased from TCI chemicals for the use as a photoinitiator and optical blocker. Red and green dyes were purchased from SewonAMT.

2. Resin Formulation and DLP 3D Printing

All resin compositions are prepared by mixing the basic composition and monomer acrylate in a weight ratio of 6 : 4. The basic composition is a 48.98 : 50 : 0.75 : 0.27 weight ratio mixture of UA, IBA, BAPO, and TBT. Five resin compositions were prepared, and the contents of each composition are summarized in Table 1. The first composition in the table, B-PD, contains a 1 : 1 mixture of PETA and DPGDA as a monomer acrylate. The remaining four compositions contain a monomer acrylate of ETPTA, TMPTA, DPGDA, or HBA. Resins were prepared by macroscopic mixing with a wood stick and microscopic mixing with a vortex mixer and ultrasonicator and stored overnight in a dark room to remove air bubbles.

3. DLP 3D Printing

A DLP 3D printer (Wanhao, D7 plus) having a 405 nm UV light source (30 W) was used, and the slicing operation for printing was performed using software, Chitubox, provided by the vendor. The printing layer thickness was set to 50 μm, and each layer was exposed to UV for 10 s with the intensity of 720 mW/cm^2. Typically, 3D printing was performed after filling the vat with 100 ml of resin. In the case of multi-material printing, the other layer was printed after the vat was replaced with the other resin. After the vat was changed, the z-axis zero was newly set to compensate for the thickness of the first layer. The resin wetted on the surface of a first layer was removed with a soft cloth to prevent the second vat contamination. For high printing resolution and enhanced printing efficiency, DLP 3D printing only provides partial cross-linking to the extent of maintaining shape, and complete cross-linking is obtained in the post-curing. Therefore, printed products are post-cured for 1 hour to cross-link the unreacted acrylates completely after washing with ethanol. 365 nm UV was chosen for post-curing with a high efficiency because BAPO's absorption intensity is 30% higher than 405 nm UV. The product after 3D printing is almost flat, but excessive post-curing of certain surfaces causes warpage. Alternative crosslinking each of the upper and lower surfaces for 15 minutes twice avoided the unwanted warpage. The UV light source chosen for post-curing was 365 nm UV LED (SOLIS, Thorlabs) due to BAPO's higher absorption at 365 nm than 405 nm. Since there is a trade-off between the effects of the BAPO's degree of absorption and the penetration depth of UV, it is expected that the wavelength-dependent cross-linking efficiency depends on the sample thickness. However, as long as the printed products are relatively thin like dog bone specimens, 365 nm UV is regarded more suitable for complete cross-linking and thus used in this study.

4. Characterization

The specimen for a tensile test was prepared in the form of a dog bone according to ASTM D638IV. Single material specimens were printed with a thickness of 3.4 mm, and multi-material specimens were printed so that both materials had the same thickness of 1.7 mm each. The tensile test was performed using a Universal Testing Machine (UTM, AG-Xplus, Shimadzu), and a strain rate of

Table 1. Summary of content and mechanical properties of resin compositions used in this study

Resin name	Content (wt%)	Modulus (GPa)	Ultimate strength (MPa)	Elongation at break (%)
B-PD	B 40/PETA 20/DPGDA 20	1.756	61.51 MPa	6.71%
B-E3	B 40/ETPTA 40	1.478	44.21 MPa	10.19%
B-T3	B 40/TMPTA 40	1.572	51.59 MPa	6.01%
B-D2	B 40/DPGDA 40	1.212	43.43 MPa	9.65%
B-H1	B 40/HBA 40	0.002	1.73 MPa	145.75%

B: UA 48.98/IBA 50/BAPO 0.75/TBT 0.27

5 mm/min and a load cell of 50 kN were applied. At least ten samples were measured to obtain the average modulus, ultimate strength, and elongation at break for the five resin compositions, summarized in Table 1. Viscosity of resins was measured using a cone-plate rheometer (Discovery HR30, TA instrument) in the shear rate range of 0.1 to 1,000 s^{-1} at 20 °C. In the shear rate range, the viscosity was almost uniform, so we used the average value.

RESULTS AND DISCUSSION

Resin compositions for DLP 3D printing are generally composed of an oligomer, monomer, photoinitiator, and optical blocker. An oligomer is a high molecular weight acrylate having a functionality typically between 2 and 6 that plays a role in preventing distortion of the printout by minimizing volume shrinkage during cross-linking. In this experiment, a difunctional UA with molecular weight of 2,000 g/mol, which has high modulus and strength, was used as an oligomer. The viscosity of the oligomer, 10 Pa·s at 60 °C, largely exceeds the requirement for printing, 5 Pa·s at 20 °C [34]. Therefore, IBA (η~10 mPa·s at 20 °C) was used as a diluent. BAPO was used as the photoinitiator due to its high photoinitiation efficiency at the UV wavelength of a 3D printer, 405 nm. TBT was used as the optical blocker for controlling UV penetration depth. The composition containing UA, IBA, BAPO, and TBT was used as the basic composition in the entire study.

We added each, or combination of five, acrylates with different functionality to the above basic composition to control the mechanical property. The added acrylates were PETA, ETPTA, TMPTA, DPGDA, and HBA, and their functionality was 4, 3, 3, 2, and 1, respectively. The ratio of the basic composition and added acrylate was fixed at 6 : 4 by volume. The composition with the highest mechanical strength was the composition in which PETA and DPGDA were added at a ratio of 1 : 1 to the basic composition. As shown in Fig. 1, the modulus and ultimate strength of the composition were 1.756 GPa and 61.71 MPa, respectively, whereas the elongation was 6.71%. On the other hand, the composition containing the basic composition and HBA showed the lowest modulus and strength of 0.002 GPa and 1.73 MPa, while the elongation was 145.75%, showing the typical behavior of elastomers. For convenience, the resin composition containing the basic composition (B), PETA (P), and DPGDA (D) is referred to as B-PD. The resin composition containing the basic composition (B) and ETPTA (E), TMPTA (T), DPGDA (D), or HBA (H) is referred to as B-E3, B-T3, B-D2, and B-H1 by marking its functionality at the end. The resins were printed in dog bone shape and a tensile test was performed. The composition, modulus, ultimate strength, and elongation at break of the five resin compositions are summarized in Table 1.

For mechanical testing of multi-materials, a dog bone shape specimen with a thickness of half B-PD and the other half B-E3, B-T3, B-D2, or B-H1 was prepared. The first half layer was printed in a vat containing B-PD, and the last half was printed after replacement with a vat containing the other resin composition. Through the tensile test, modulus, ultimate strength, and elongation at break

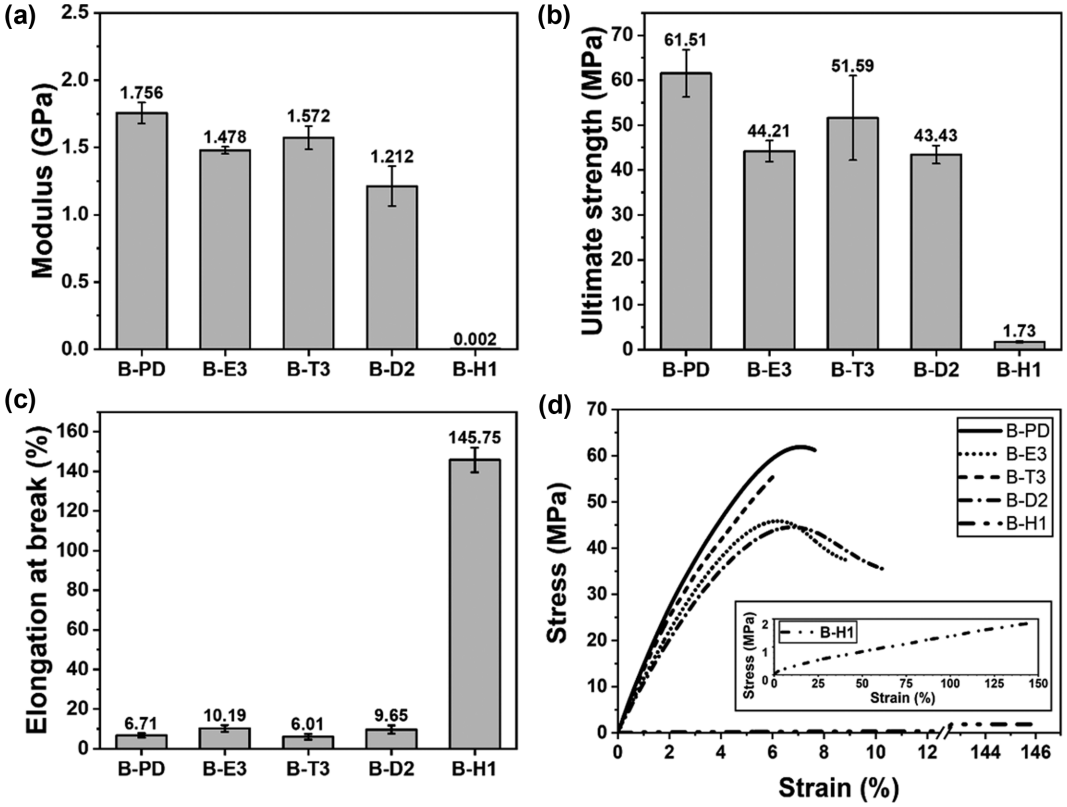

Fig. 1. (a) Modulus, (b) ultimate strength, (c) elongation at break, and (d) typical stress-strain curves for 3D printed B-PD, B-E3, B-T3, B-D2, and B-H1. Inset in (d) is enlarged stress-strain curve for B-H1. Numbers above bars are averaged values.

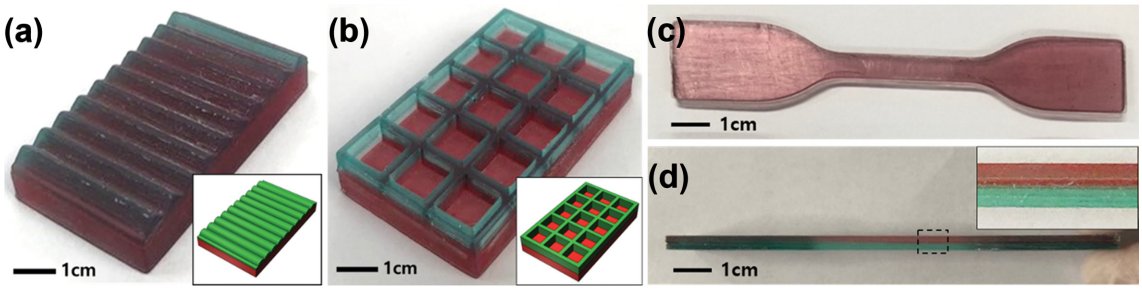

Fig. 2. 3D printed multi-material products of B-PD (red) and B-E3 (green). (a) Structures which have full and (b) partial contact between B-PD and B-E3. Insets are 3D modeled images prior to printing. (c) Top and (d) side views of a dog bone specimen for a tensile test. Inset in (d) is an enlarged image of a dashed region of gauge length.

of multi-material were analyzed. By comparing the mechanical properties of multi-material with those of constituent materials, we determined whether the mechanical properties of the multi-material were complementarily reinforced compared to those of the constituent materials.

First, we performed multi-material printing of B-PD and B-E3. Both B-E3 and B-T3 are trifunctional, but B-E3 has a flexible ethoxylate functional group, so it has a higher elongation at break. In the multi-material printing results of B-PD and B-E3, it was expected that the low elongation at break of B-PD would be compensated by the high elongation at break of B-E3. For a clear distinction between the two compositions, red and green dyes were added into B-PD and B-E3, respectively. We modeled and performed several multi-material printings as shown in Fig. 2. For example, a structure in which two materials are in full contact (Fig. 2(a)) and a structure in partial contact were fabricated (Fig. 2(b)). Since the contact surfaces of the two materials exactly match, as shown in Fig. 2, it can be confirmed that the multi-material printing is successful without alignment and distortion issues. The multi-material dog bone specimen for the tensile test was printed as shown in Fig. 2(c), and its side view image (Fig. 2(d)) is showing a clear boundary between the red and green region, showing two distinct areas of B-PD and B-E3.

The modulus of B-PD was 1.756 GPa, the highest of the five resin compositions, and the modulus of B-E3 was 1.479 GPa. In contrast, the modulus of the B-PD/B-E3 multi-material, 1.397 GPa,

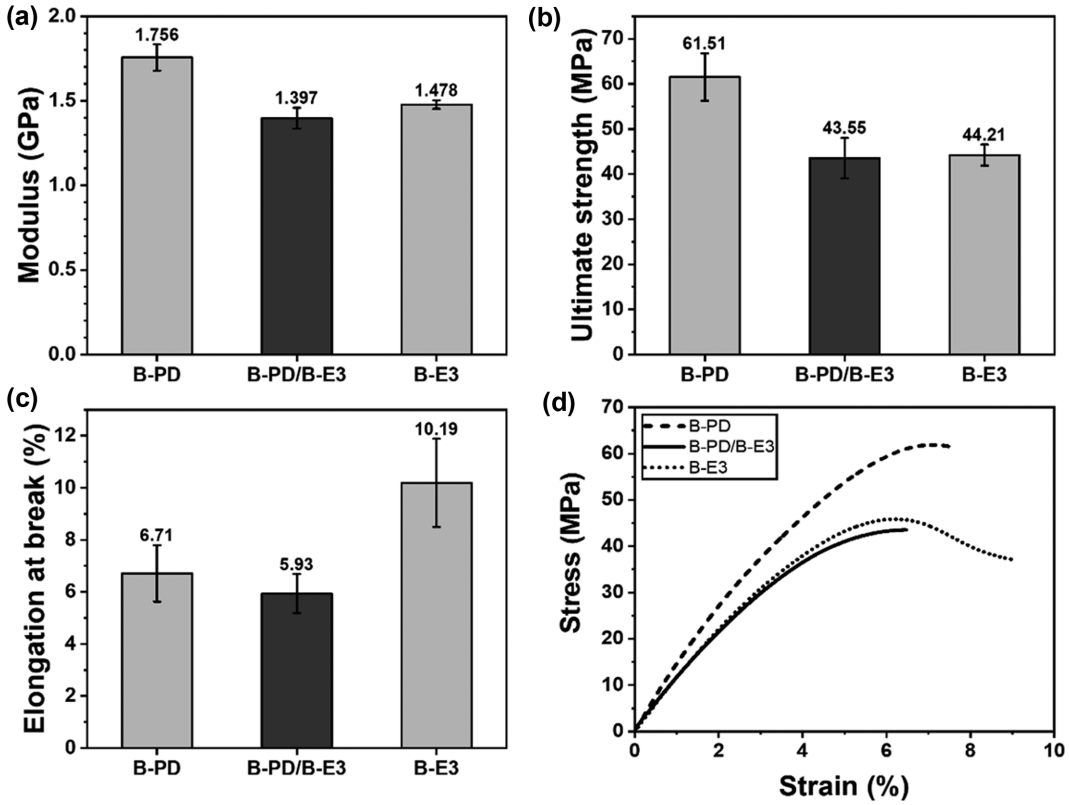

Fig. 3. (a) Modulus, (b) ultimate strength, (c) elongation at break, and (d) typical stress-strain curves for 3D printed multi-material of B-PD and B-E3 are compared with those for constituent materials.

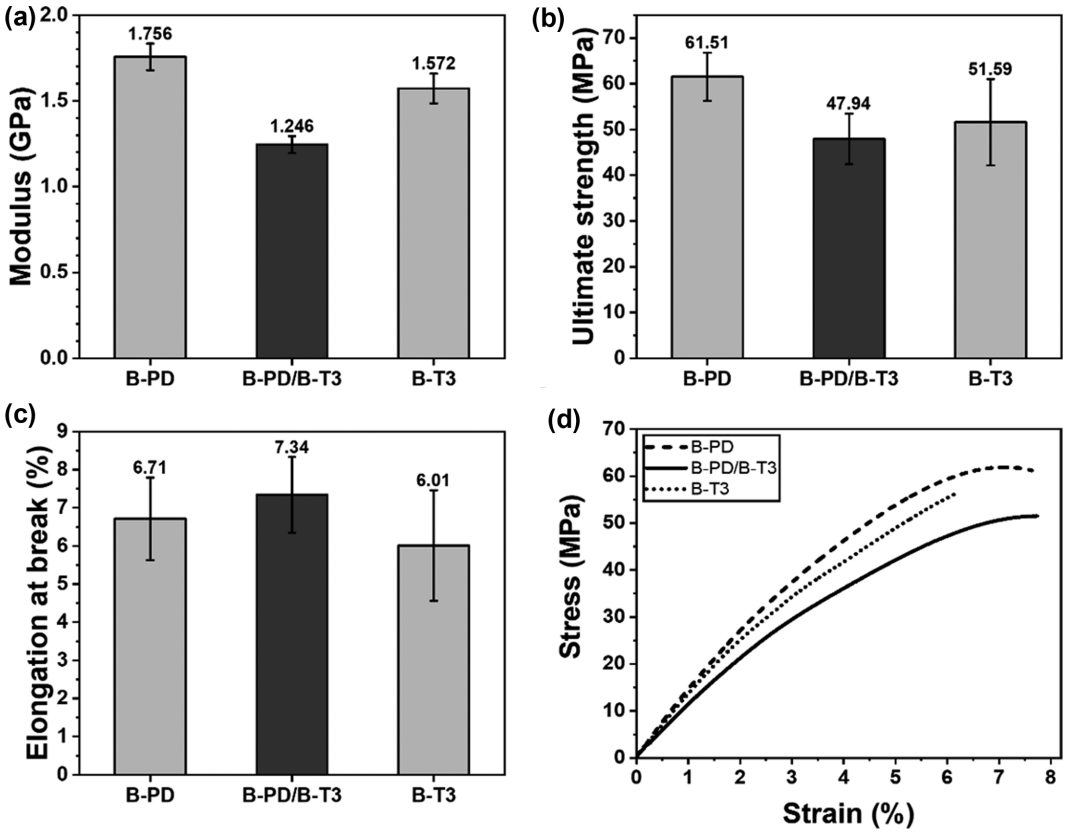

Fig. 4. (a) Modulus, (b) ultimate strength, (c) elongation at break, and (d) typical stress-strain curve for 3D printed multi-material of B-PD and B-T3 are compared with those for constituent materials.

was lower than those of the two resin compositions. In terms of ultimate strength, B-PD and B-E3 were 61.51 and 44.21 MPa, respectively. On the other hand, the ultimate strength of B-PD/B-E3 multi-material was 43.55 MPa, which was lower than that of the two resin compositions. B-PD has an elongation at break of 6.71, but B-E3 has a relatively high elongation at break of 10.19. However, the elongation at break of B-PD/B-E3 multi-material was 5.93, which was lower than that of both resins. In conclusion, the B-PD/B-E3 multi-material showed lower values in those three properties, modulus, ultimate strength, and elongation at break, than constituent materials. The typical stress-strain curve of B-PD/B-E3 multi-material was compared with those of constituent materials as shown in Fig. 3(a). B-PD was broken soon after reaching the peak, while B-E3 elongated even after the peak. On the other hand, the curve of the B-PD/B-E3 multi-material was broken near the apex and showed a smaller elongation at break than that of the B-PD. And the curve was located below the curves of two constituent materials through all strain regions.

We performed the same experiment with the B-T3 resin, containing TMPTA that is trifunctional the same as ETPTA. Though flexible ethoxylate group of ETPTA imparts high elongation, its hydrophilicity is detrimental to adhesion due to non-preferred wetting because all other materials are hydrophobic. TMPTA has a similar structure to ETPTA, but does not have ethoxylate groups. Therefore, B-PD/B-T3 multi-material is expected to show enhanced wetting and thus better adhesion than B-PD/B-E3 multi-material. However, both modulus and ultimate tensile strength were lower than those of constituent materials. B-PD and B-T3 were highly brittle with elongation at break of 6.71 and 6.01, respectively, and B-PD/B-T3 multi-material showed 7.34, higher than B-PD and B-T3 but still very low. The typical stress-strain curve for B-PD/B-T3 multi-material was compared with constituent materials as shown in Fig. 4(d). All of B-PD, B-T3, and B-PD/B-T3 showed highly brittle characteristics, and elongation at break of B-PD/B-T3 was slightly higher than constituent materials. B-PD/B-E3 multi-material was expected to show enhanced mechanical properties by improved wetting, but the B-PD/B-T3 curve was located below the curve of constituent materials through all strain regions.

We next performed B-PD/B-D2 multi-material printing. The B-PD/B-D2 multi-material exhibited improved modulus, ultimate strength, and elongation at break than constituent materials. The modulus of B-PD/B-D2 is 1.765 GPa, which is higher than the modulus of B-PD that is the highest among all constituent materials. In addition, the ultimate strength is 55.58 MPa, which exceeds the average ultimate strength of constituent materials, 52.37 MPa, by 6.1%. The elongation at break of B-PD/B-D2 was 8.94%, which was 9.3% higher than the average elongation at break of two materials, 8.18%. A typical stress-strain curve of B-PD/B-D2 is shown in Fig. 5(d). The curve of B-PD/B-D2 is located between curves of constituent materials in all strain regions, and the three mechanical properties exhibit a complementary reinforcement that shows improved characteristics over the average properties of each material.

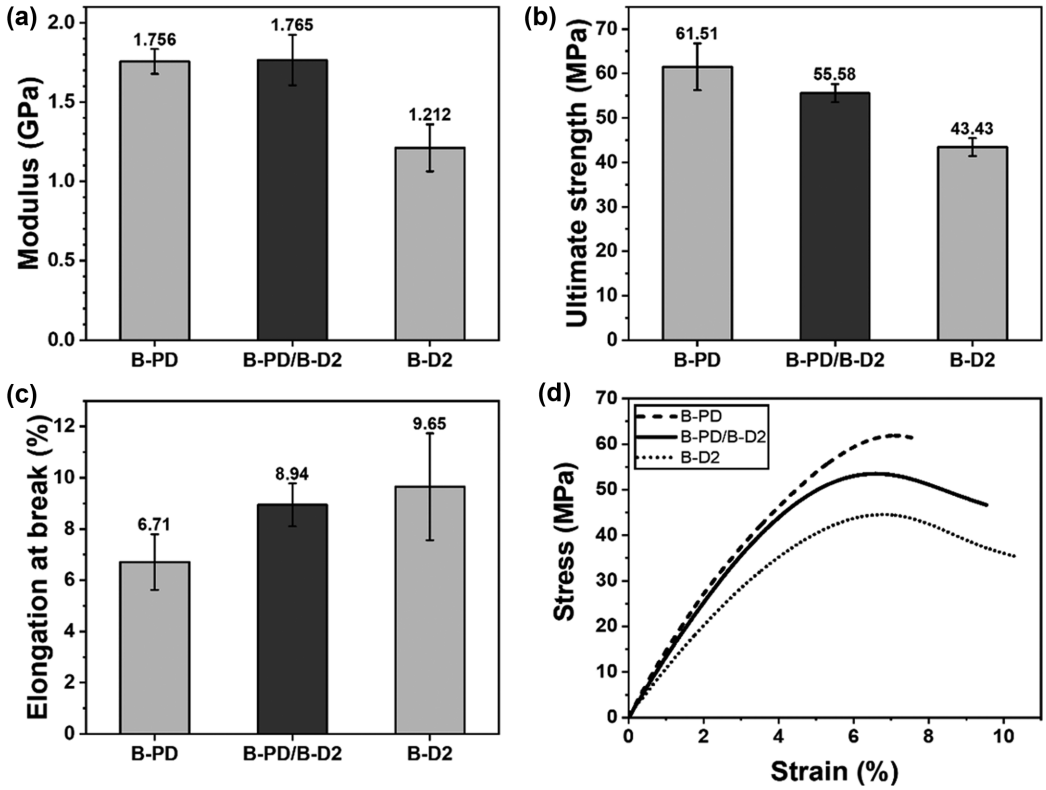

Fig. 5. (a) Modulus, (b) ultimate strength, (c) elongation at break, and (d) typical stress-strain curve for 3D printed multi-material of B-PD and B-D2 are compared with those for constituent materials.

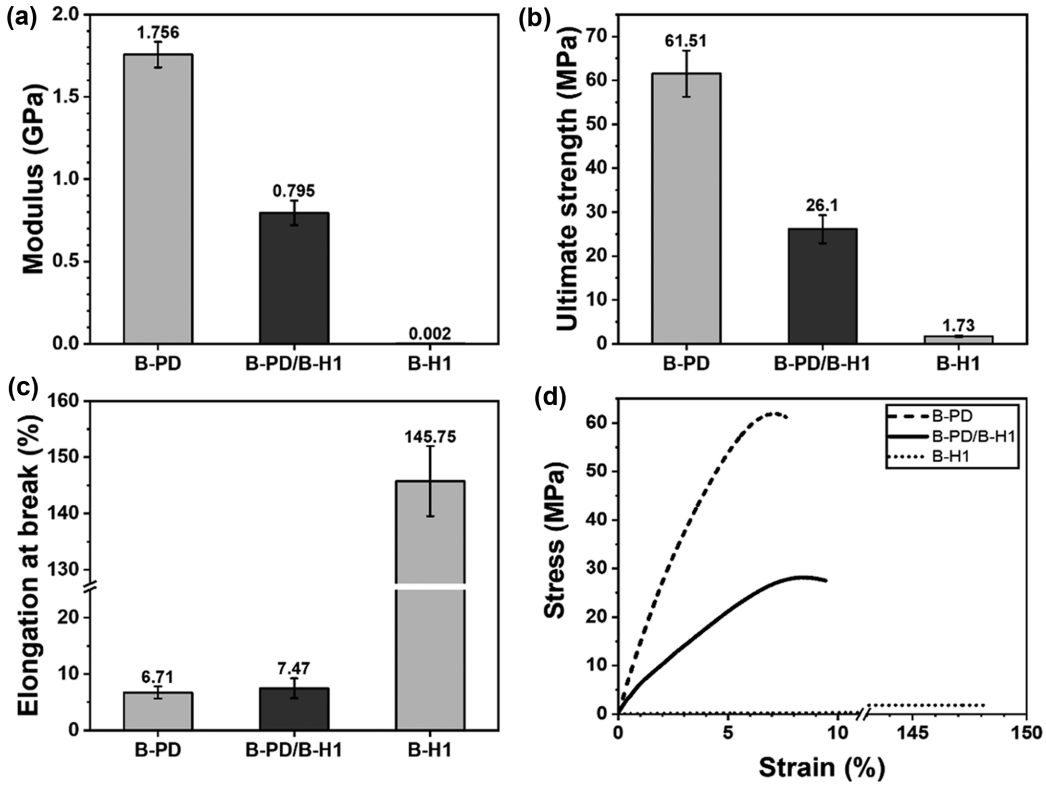

Fig. 6. (a) Modulus, (b) ultimate strength, (c) elongation at break, and (d) typical stress-strain curve for 3D printed multi-material of B-PD and B-H1 are compared with those for constituent materials.

Finally, we performed B-PD/B-H1 multi-material printing. The average modulus of B-PD/B-H1 was 0.795 GPa (Fig. 6(a)), which was about 9.5% lower than the average modulus of constituent materials, 0.879 GPa. The average ultimate strength of B-PD/B-H1 was 26.1 MPa (Fig. 6(b)), 17.5% lower than the average ultimate strength of two materials, 31.62 MPa. The average elongation at break of B-PD/B-H1 was 7.47% (Fig. 6(c) and (d)), much lower than that of B-H1 but increased by 11.3% than that of B-PD. The average modulus and ultimate strength of B-PD/B-H1 were close to the average of the modulus and ultimate strength of constituent materials, while the elongation at break was significantly less than the average. The low elongation at break can be attributed to the propagation of cracks from the B-PD part to B-H1 through the interface. Since the B-PD printing product is brittle, cracks likely occurred in the strain exceeding B-PD's elongation at break. The crack of the B-PD part would have easily propagated to the soft B-H1 part due to the dense interfacial adhesion between them, and the multi-material was broken due to the concentrated stress on the crack. We speculate that elongation at break can be improved by placing a protective layer between B-PD and B-H1.

In conclusion, B-D2 and B-H1 containing relatively lower functional monomers showed a better complementary effect in mechanical properties than B-E3 and B-T3 in multi-material 3D printing. We compared the fracture surfaces of the B-PD/B-D2 and B-PD/B-E3 multi-materials to figure out the cause of this difference in mechanical properties (Fig. 7). In the case of the B-PD/B-D2 multi-material, the surface texture is uniform throughout the fracture surface, as shown in Fig. 7(a). That means that the two materials reached fracture at the same time without losing interfacial adhesion. On the other hand, B-PD/B-E3 multi-material showed a marked difference in the surface texture for the two materials, as shown in Fig. 7(b). The B-PD surface has a rough surface similar to the fracture surface of the B-PD/B-D2 multi-material, whereas the B-E3 surface has a smooth surface as evidenced by uniform surface reflection. For ductile fracture of polymer, dimples are generated by fracture of microvoids induced by craze, which causes a rough surface [35]. On the other hand, a smooth surface of B-E3 is caused by a brittle fracture without craze, so B-E3 hardly causes plastic deformation and is fractured before fracture of B-PD. Therefore, it can be considered that B-PD/B-E3 multi-materials have poor interfacial adhesion compared to B-PD/B-D2, which causes little or almost no complementary effect on mechanical properties.

To determine the cause of this difference in interfacial adhesion strength, we compared the modulus and tensile strength of multi-materials. We depicted normalized modulus change and normalized tensile strength change in Fig. 7(a) and (b). The normalized change, C_N, was calculated using Eq. (1).

$$C_N = \frac{val_M - val_L}{val_H - val_L} \tag{1}$$

where val_M, val_H, and val_L are modulus (or tensile strength) for multi-material, higher modulus (or tensile strength) material, and lower modulus (or tensile strength) material. The normalized modulus of positive 0.5 means that the multi-material has the average modulus (or tensile strength) of the constituent materials. The normalized modulus of B-PD/B-D2 exceeded 1.0, and that of B-PD/B-H1 was slightly less than 0.5 (Fig. 8(a)). On the other hand, the normalized moduli of B-PD/B-E3 and B-PD/B-T3 were negative, which means the modulus of multi-material is smaller than that of each material. Similarly, the normalized tensile strength of B-PD/B-D2 and B-PD/B-H1 was higher and slightly less than 0.5, but B-PD/B-E3 and B-PD/B-T3 were negative (Fig. 8(b)). The tendency is exactly the opposite to the tendency of viscosity of resins (Fig. 8(c)). As shown in Fig. 8, higher functional acrylates, B-E3 and B-T3, that showed negative changes have a higher viscosity of 0.384 and 0.526 mPa·s, whereas lower functional acrylates, B-D2 and B-H1, that showed positive changes higher or near than 0.5 have a lower viscosity of 0.129 and 0.098 mPa·s. We speculate that lower viscosity helps improve interfacial adhesion of multi-material. High functional acrylates are usually more viscous [34,36] and generally cause early gelation and vitrification, thus lowering the final degree of polymerization [34]. On the other hand, low functional acrylates are usually less viscous and allow a sufficiently high degree of polymerization before vitrification occurs by slowing the gelation, thus improving interfacial adhesion by promoting polymerization at the interface [34]. In addition, the low viscosity of resin

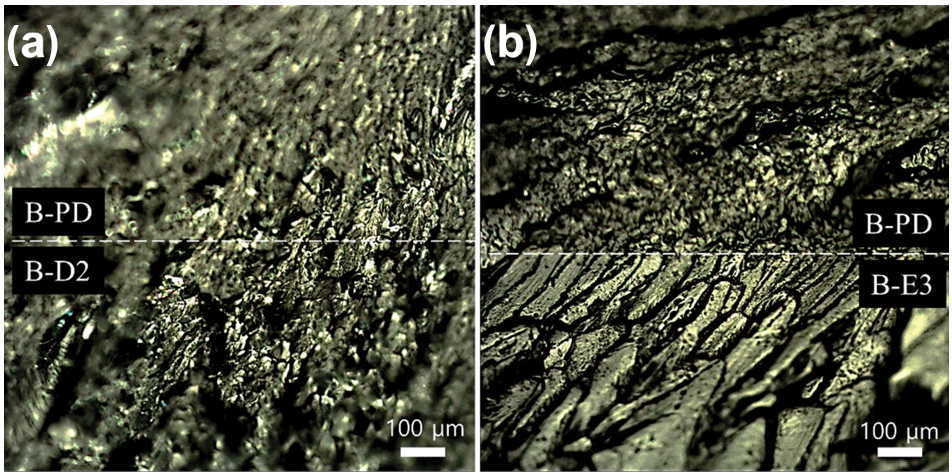

Fig. 7. Optical microscope images of fracture surface of (a) B-PD/B-D2 and (b) B-PD/B-E3.

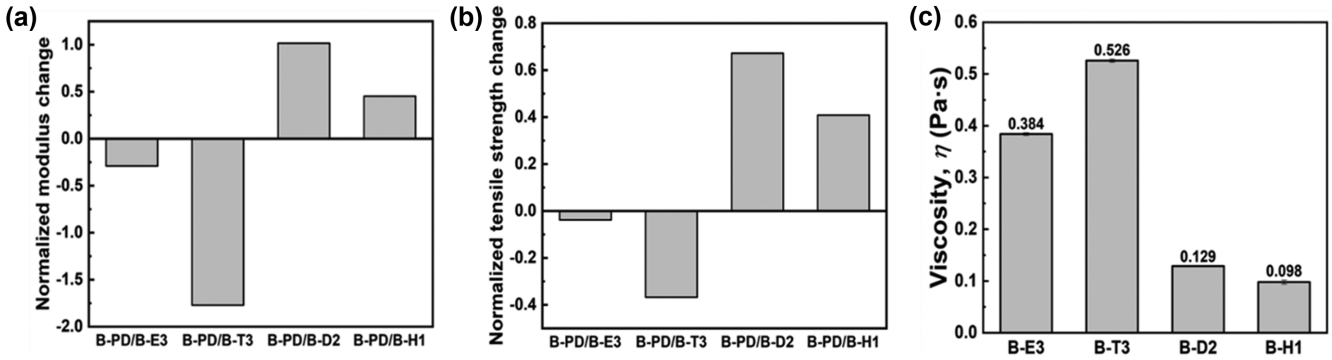

Fig. 8. (a) Normalized modulus change and (b) normalized tensile strength change of B-PD/B-E3, B-PD/B-T3, B-PD/B-D2, and B-PD/B-H1. (c) Viscosity of B-PD, B-E3, B-T3, B-D2, and B-H1.

helps improve cross-linking efficiency and uniformity by accelerating the movement of fresh acrylates to the area of UV curing. In summary, improved adhesion was achieved by printing a resin containing low functional acrylate on a pre-printed layer, which contributes to the fabrication of 3D printing-based multi-material parts supplemented with the advantages in mechanical property of each material. In addition, DLP 3D printing has the advantage of having an elaborate layer resolution of less than 50 μm, enabling the development of robust engineering parts with a fine resolution that is not possible with the extrusion-based 3D printing method, which will significantly expand the industrial application of 3D printing. Though we demonstrate only z-directionally variable multi-materials here, developing a new 3D printing platform that manipulates exposure direction freely [37] will enable multi-directionally variable multi-materials.

CONCLUSIONS

We formulated five different resin compositions for DLP 3D printing containing acrylates of varying functionality and successfully performed multi-material printing. B-PD, which shows the highest modulus and ultimate strength, was printed as the first half layer, and the other half layer of B-E3, B-T3, B-D2, or B-H1 containing acrylates with functionality between 1 and 3 was printed for mechanical testing of multi-materials. B-PD/B-E3 and B-PD/B-T3 multi-materials showed reduced mechanical properties than constituent materials except for elongation at break of B-PD/B-T3. On the other hand, the B-PD/B-D2 and B-PD/B-H1 multi-materials exhibited composite behavior with average mechanical properties of constituent materials. This improvement in mechanical properties becomes possible due to improvement in adhesion. Observing the fracture surface of B-PD/B-D2 confirmed that B-PD/B-D2 shows uniform texture throughout the fracture surface, which evidences reliable interfacial adhesion between B-PD and B-D2. The reliable adhesion is enabled by low functional acrylate monomer by promoting polymerization reaction at the interface due to delayed gelation and facilitating the migration of fresh acrylates to the UV exposure area due to low viscosity. This approach to provide reliable interfacial adhesion in DLP 3D printing will enable the development of sophisticated multi-material engineering parts with robust mechanical properties, contributing to the expansion of 3D printing into the industrial field.

NOTES

The authors declare no competing financial interest.

ACKNOWLEDGEMENT

This research was supported by Kumoh National Institute of Technology (2020-022-300-01).

REFERENCES

1. X. Wang, M. Jiang, Z. Zhou, J. Gou and D. Hui, *Compos. B. Eng.*, **110**, 442 (2017).
2. T. D. Ngo, A. Kashani, G. Imbalzano, K. T. Q. Nguyen and D. Hui, *Compos. B. Eng.*, **143**, 172 (2018).
3. S. C. Ligon, R. Liska, J. Stampfl, M. Gurr and R. Mülhaupt, *Chem. Rev.*, **117**, 10212 (2017).
4. M. Vaezi, S. Chianrabutra, B. Mellor and S. Yang, *Virtual Phys. Prptotyp.*, **8**, 19 (2013).
5. A. Bandyopadhyay and B. Heer, *Mater. Sci. Eng. R Rep.*, **129**, 1 (2018).
6. S. Derakhshanfar, R. Mbeleck, K. Xu, X. Zhang, W. Zhong and M. Xing, *Bioact. Mater.*, **3**, 144 (2018).
7. W. Liu, Y. S. Zhang, M. A. Heinrich, F. D. Ferrari, H. L. Jang, S. M. Bakht, M. M. Alvarez, J. Yang, Y.-C. Li, G. T. Santiago, A. K. Miri, K. Zhu, P. Khoshakhlagh, G. Prakash, H. Cheng, X. Guan, Z. Zhong, J. Ju, G. H. Zhu, X. Jin, S. R. Shin, M. R. Dokmeci and A. Khademhosseini, *Adv. Mater.*, **29**, 1604630 (2017).
8. M. Rafiee, R. D. Farahani and D. Therriault, *Adv. Sci.*, **7**, 1902307 (2020).
9. S.-J. Jeon, A. W. Hauser and R. C. Hayward, *Acc. Chem. Res.*, **50**, 161 (2017).
10. S. J. Keating, M. I. Gariboldi, W. G. Patrick, S. Sharma, D. S. Kong and N. Oxman, *PLoS One*, **11**, e0160624 (2016).
11. A. Cazón-Martín, M. Iturrizaga-Campelo, L. Matey-Munoz, M. I. Rodríguez-Ferradas, P. Morer-Camo and S. Ausejo-Munoz, *Proc. Inst. Mech. Eng. Part P J. Sport. Eng. Technol.*, **233**, 160 (2019).
12. J. P. Moore and C. B. Williams, *Rapid Prototyp. J.*, **21**, 675 (2015).
13. T. S. Lumpe, J. Mueller and K. Shea, *Mater. Des.*, **162**, 1 (2019).

14. Z. Jiang, B. Diggle, M. L. Tan, J. Viktorova, C. W. Bennett and L. A. Connal, *Adv. Sci.*, **7**, 2001379 (2020).
15. D. Popescu, A. Zapciu, C. Amza, F. Baciu and R. Marinescu, *Polym. Test.*, **69**, 157 (2018).
16. L. R. Lopes, A. F. Silva and O. S. Carneiro, *Addit. Manuf.*, **23**, 45 (2018).
17. C. Bellehumeur, L. Li, Q. Sun and P. Gu, *J. Manuf. Process*, **6**, 170 (2004).
18. D. Espalin, J. A. Ramirez, F. Medina and R. Wicker, *Rapid Prototyp. J.*, **20**, 236 (2014).
19. L. Li, Q. Lin, M. Tang, A. J. E. Duncan and C. Ke, *Chem. Eur. J.*, **25**, 10768 (2019).
20. P. Jiang, Z. Ji, X. Zhang, Z. Liu and X. Wang, *Prog. Addit. Manuf.*, **3**, 65 (2018).
21. V. G. Rocha, E. Saiz, L. S. Tirichenko and E. García-Tuñón, *J. Mater. Chem. A*, **8**, 15646 (2020).
22. K. Tian, Z. Suo and J. J. Vlassak, *ACS Appl. Mater. Interfaces*, **12**, 31002 (2020).
23. A. Bagheri and J. Jin, *ACS Appl. Polym. Mater.*, **1**, 593 (2019).
24. J. Zhang and P. Xiao, *Polym. Chem.*, **9**, 1530 (2018).
25. H. Quan, T. Zhang, H. Xu, S. Luo, J. Nie and X. Zhu, *Bioact. Mater.*, **5**, 110 (2020).
26. Q. Ge, Z. Li, Z. Wang, K. Kowsari, W. Zhang, X. He, J. Zhou and N. X. Fang, *Int. J. Extrem. Manuf.*, **2**, 022004 (2020).
27. J. Borrello, P. Nasser, J. C. Iatridi and K. D. Costa, *Addit. Manuf.*, **23**, 374 (2018).
28. Q. Ge, A. H. Sakhaei, H. Lee, C. K. Dunn, N. X. Fang and M. L. Dunn, *Sci. Rep.*, **6**, 31110 (2016).
29. D. Han, C. Yang, N. X. Fang and H. Lee, *Addit. Manuf.*, **27**, 606 (2019).
30. B. Khatri, M. Frey, A. Raouf-Fahmy, M.-V. Scharla and T. Hanemann, *Micromachines*, **11**, 532 (2020).
31. T. Maruyama, H. Hirata, T. Furukawa and S. Maruo, *Opt. Mater. Express*, **10**, 2522 (2020).
32. B. Zhang, S. Li, H. Hingorani, A. Serjouei, L. Larush, A. A. Pawar, W. H. Goh, A. H. Sakhaei, M. Hashimoto, K. Kowsari, S. Magdassi and Q. Ge, *J. Mater. Chem. B*, **6**, 3246 (2018).
33. C. Creton, *MRS Bull.*, **28**, 434 (2003).
34. G. Taormina, C. Sciancalepore, M. Messori and F. Bondioli, *J. Appl. Biomater. Funct. Mater.*, **16**, 151 (2018).
35. W. T. Becker and R. J. Shipley, *Failure analysis and prevention*, ASM International, Materials Park (2002).
36. S. Ebnesajjad, *Handbook of adhesives and surface preparation: Technology, applications and manufacturing*, William Andrew, Amsterdam (2011).
37. B. E. Kelly, I. Bhattacharya, H. Heidari, M. Shusteff, C. M. Spadaccini and H. K. Taylor, *Science*, **363**, 1075 (2019).